ELSEVIER

Comput. Methods Appl. Mech. Engrg. 143 (1997) 49–67

Computer methods in applied mechanics and engineering

A finite element formulation for incompressible flow problems using a generalized streamline operator

Marcela A. Cruchaga*, Eugenio Oñate

International Center for Numerical Methods in Engineering, E.T.S. d'Enginyers de Camins, Canals i Ports,

Received 23 May 1995; revised 21 February 1996

Abstract

A finite element formulation for solving incompressible flow problems is presented. In this paper, the generalized streamline operator presented by Hughes et al. (Comput. Methods Appl. Mech. Engrg. (1986) 58 305–328) for compressible flows is adapted to the incompressible Navier–Stokes equations. This new methodology allows the use of equal order interpolation for the unknowns of the problem: velocity and pressure. In this context, the definition of the 'upwinding tensor' does not require parameters defined outside this model. This formulation has been checked in classical tests with satisfactory results. Finally, a moving surface problem (Cruchaga et al., Comput. Numer. Methods Engrg. (1986) 59: 85–99) is also presented.

1. Introduction

In the present work a numerical formulation able to deal with incompressible flow problems is developed. The difficulties in the numerical solution of the Navier–Stokes equations are well known: oscillations appear in the results when the convective term becomes relevant and mathematical requirements impose restrictions on the choice of the discrete approximation functions although, however, a recent formulations allow to overcome such restrictions [1–4]. In the context of the finite element method, a Galerkin Least Squares type formulation using a generalized streamline operator [5] applied to the incompressible flow case is presented. This technique enables the use of equal interpolation function for the primitive variables of the problem: velocity and pressure. In this case, the standard penalization methods necessary to fulfil the incompressibility equation are not required.

The choice of the upwinding parameters, crucial to obtain stable and convergent formulations, involves several works and discussions [4,6–9]. In this paper, a new design of these parameters is obtained in the framework of the generalized streamline operator (GSO) presented by Hughes et al. [5] extending the methodology initially developed for compressible flows [9]. The GSO consists, basically, in writing the Navier–Stokes equations in the advective eigenvector system. In this basis, the diffusivity matrix is lumped leading to an uncoupled governing equations (considering a constant viscosity) and, therefore, the computation of the upwinding coefficient at each direction can be performed in the standard manner. Further, a diagonal upwinding tensor is obtained and, transforming this tensor back to the original system, the weighting perturbation function can be defined.

The governing equations for the incompressible flow problem and the corresponding weak form are

* Corresponding author.

PII S0045-7825(96)001149-8

described in Section 2. In Section 3, the methodology followed to compute the upwinding tensor is presented. It is important to note that this tensor does not require tuning parameters defined outside this model. Further, the resulting finite element formulation is briefly described in Section 4.

A brief description of the numerical strategy is performed in Section 5 where an incremental-iterative solution strategy has been implemented such that the convergence criterion is written in terms of the norm of the residual vector.

In Section 6, the driven cavity flow problem is analysed at different Reynolds' numbers and a comparative analysis with other techniques is performed. The backward-facing step flow is also studied in order to compare with experimental results. Finally, a two-liquid interface problem is solved using the presented methodology.

2. Governing equations and weak form

The basic formulation for incompressible flow problems considering a Newtonian fluid are described by the Cauchy's equation of motion and the continuity equation which are written in Cartesian components as

$$\rho \frac{\partial u_i}{\partial t} + \rho \frac{\partial u_i}{\partial x_j} u_j + \frac{\partial p}{\partial x_i} - \frac{\partial (2\mu \varepsilon_{ij})}{\partial x_j} = \rho b_i \quad \text{in } \Omega \times [0, T] \tag{1}$$

$$\frac{\partial u_i}{\partial x_i} = 0 \quad \text{in } \Omega \times [0, T] \tag{2}$$

where Ω is an arbitrary open bounded domain with smooth boundary Γ, $[0, T]$ is the time interval of interest, $i = 1, \ldots, n_{\text{dim}}$ (n_{dim} being the spatial dimension), u_i is the i component of the velocity vector, p is the pressure, b_i is the i component of the specific body force vector, μ is the dynamic viscosity and ρ is the density.

These equations can be written in the generalized convection-diffusion system as [1, 10]

$$\boldsymbol{M} \cdot \dot{\boldsymbol{U}} + \boldsymbol{A} : \boldsymbol{L} - \boldsymbol{\nabla} \cdot (\boldsymbol{K} : \boldsymbol{L}) = \boldsymbol{F} \tag{3}$$

and in indicial notation as

$$M_{im} \dot{u}_m + A_{imn} L_{mn} - \nabla_j K_{jimn} L_{mn} = F_i \tag{4}$$

where

- $\boldsymbol{U}$ is the unknown vector, $\boldsymbol{U} = [u_1, u_2, u_3, u_4]$ with $u_4 = p$. Now, $i = 1, \ldots, n_{\text{dim}} + 1$, $m = 1, \ldots, n_{\text{dim}} + 1$, $n = 1, \ldots, n_{\text{dim}}$ and $j = 1, \ldots, n_{\text{dim}}$.
- $\boldsymbol{A} = A_{imn}$ is the generalized advection tensor. For a fixed value of $n = \bar{n}$, $\boldsymbol{A}_{\bar{n}} = [A_{im\bar{n}}]$ is defined as

$$\boldsymbol{A}_1 = \begin{bmatrix} \rho u_1 & 0 & 0 & 1 \\ 0 & \rho u_1 & 0 & 0 \\ 0 & 0 & \rho u_1 & 0 \\ 1 & 0 & 0 & 0 \end{bmatrix} \quad \boldsymbol{A}_2 = \begin{bmatrix} \rho u_2 & 0 & 0 & 0 \\ 0 & \rho u_2 & 0 & 1 \\ 0 & 0 & \rho u_2 & 0 \\ 0 & 1 & 0 & 0 \end{bmatrix} \quad \boldsymbol{A}_3 = \begin{bmatrix} \rho u_3 & 0 & 0 & 0 \\ 0 & \rho u_3 & 0 & 0 \\ 0 & 0 & \rho u_3 & 1 \\ 0 & 0 & 1 & 0 \end{bmatrix} \tag{5}$$

- $\boldsymbol{K} = K_{jimn}$ is a generalized diffusion tensor. For a fixed value of $n = \bar{n}$ and $j = \bar{j}$, $\boldsymbol{K}_{\bar{j}\bar{n}} = [K_{\bar{j}im\bar{n}}]$ is defined as

$$\boldsymbol{K}_{11} = \begin{bmatrix} 2\mu & 0 & 0 & 0 \\ 0 & \mu & 0 & 0 \\ 0 & 0 & \mu & 0 \\ 0 & 0 & 0 & 0 \end{bmatrix} \quad \boldsymbol{K}_{12} = \begin{bmatrix} 0 & \mu & 0 & 0 \\ 0 & 0 & 0 & 0 \\ 0 & 0 & 0 & 0 \\ 0 & 0 & 0 & 0 \end{bmatrix} \quad \boldsymbol{K}_{13} = \begin{bmatrix} 0 & 0 & \mu & 0 \\ 0 & 0 & 0 & 0 \\ 0 & 0 & 0 & 0 \\ 0 & 0 & 0 & 0 \end{bmatrix} \tag{6.1}$$

$$\boldsymbol{K}_{21}=\begin{bmatrix}0&0&0&0\\ \mu&0&0&0\\ 0&0&0&0\\ 0&0&0&0\end{bmatrix}\quad \boldsymbol{K}_{22}=\begin{bmatrix}\mu&0&0&0\\ 0&2\mu&0&0\\ 0&0&\mu&0\\ 0&0&0&0\end{bmatrix}\quad \boldsymbol{K}_{23}=\begin{bmatrix}0&0&0&0\\ 0&0&\mu&0\\ 0&0&0&0\\ 0&0&0&0\end{bmatrix} \tag{6.2}$$

$$\boldsymbol{K}_{31}=\begin{bmatrix}0&0&0&0\\ 0&0&0&0\\ \mu&0&0&0\\ 0&0&0&0\end{bmatrix}\quad \boldsymbol{K}_{32}=\begin{bmatrix}0&0&0&0\\ 0&0&0&0\\ 0&\mu&0&0\\ 0&0&0&0\end{bmatrix}\quad \boldsymbol{K}_{33}=\begin{bmatrix}\mu&0&0&0\\ 0&\mu&0&0\\ 0&0&2\mu&0\\ 0&0&0&0\end{bmatrix} \tag{6.3}$$

- $\boldsymbol{L}$ is the spatial gradient tensor of the unknown defined as $L_{mn}=\partial u_m/\partial x_n$.
- $\boldsymbol{\nabla}$ is the gradient operator $\nabla_j(\cdot)=\partial(\cdot)/\partial x_j$.
- $\boldsymbol{M}$ is the generalized mass tensor:

$$\boldsymbol{M}=\begin{bmatrix}\rho&0&0&0\\ 0&\rho&0&0\\ 0&0&\rho&0\\ 0&0&0&0\end{bmatrix} \tag{7}$$

- $\boldsymbol{F}$ is the body force vector.

$$\boldsymbol{F}=[\rho b_1,\rho b_2,\rho b_3,0] \tag{8}$$

The formal problem consists of finding $\boldsymbol{U}$ verifying the system (3) such that

$$\mathcal{R}(\boldsymbol{U})\equiv\boldsymbol{M}\cdot\dot{\boldsymbol{U}}+\boldsymbol{A}:\boldsymbol{L}-\boldsymbol{\nabla}\cdot(\boldsymbol{K}:\boldsymbol{L})-\boldsymbol{F}=\boldsymbol{0}\quad\text{in }\Omega\times[0,T] \tag{9}$$

subject to appropriate boundary and initial conditions [2,10–12]:

$$\boldsymbol{U}=(\bar{u}_1,\bar{u}_2,\bar{u}_3,u_4)\quad\text{in }\Gamma_u\times[0,T] \tag{10.1}$$

$$\boldsymbol{U}=(u_1,u_2,u_3,\bar{u}_4)\quad\text{in }\Gamma_p\times[0,T] \tag{10.2}$$

$$(\boldsymbol{K}:\boldsymbol{L})\cdot\boldsymbol{n}=\boldsymbol{H}\quad\text{in }\Gamma_H\times[0,T] \tag{10.3}$$

$$\boldsymbol{U}_0=\boldsymbol{U}(\boldsymbol{x},0)\quad\text{in }\Omega \tag{10.4}$$

where $\boldsymbol{H}$ is the prescribed deviatoric stress tensor, $\boldsymbol{n}$ is the outward unit vector normal to Γ_H. Besides, $\Gamma_u,\Gamma_p,\Gamma_H$ are the parts of Γ on which the velocity, the pressure and the deviatoric part of the stress tensor are prescribed, respectively ($\Gamma_u\cup\Gamma_H=\Gamma$ and $\Gamma_u\cap\Gamma_H=\emptyset$); see Fig. 1.

In order to obtain the weak form of this initial boundary value problem, the perturbation function added to the standard Galerkin weighting function is defined as [5]

$$\boldsymbol{P}(\boldsymbol{\Psi})=\boldsymbol{\tau}\cdot\mathcal{R}(\boldsymbol{\Psi}) \tag{11}$$

where $\mathcal{R}$ defined in Eq. (9) is applied to the test function $\boldsymbol{\Psi}$ and $\boldsymbol{\tau}$ is the second-order 'upwinding

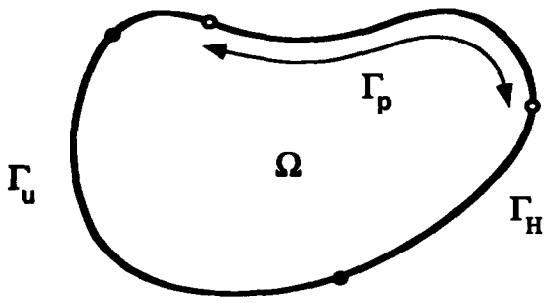

Fig. 1. Arbitrary domain and its boundary.

tensor' that will be defined in Section 3 ($\tau = \tau_{iq}$, with $i = 1, \ldots, n_{\dim} + 1$ and $q = 1, \ldots, n_{\dim} + 1$). In the present work, only the convective part of the perturbation function is used. Therefore, the weighting function is time-independent, the effect of the diffusive term involving second derivatives of the unknowns is neglected, and the source term does not depend on the variables of the problem. Accordingly, the perturbation function is written as [5,10]

$$\boldsymbol{P}(\boldsymbol{\Psi}) = \boldsymbol{\tau} \cdot (\boldsymbol{A} : \boldsymbol{L}(\boldsymbol{\Psi})) = \tau_{iq} A_{qmn} L_{mn}(\boldsymbol{\Psi}) = \beta_{imn} L_{mn}(\boldsymbol{\Psi}) = \beta : L(\boldsymbol{\Psi}) \tag{12}$$

Finally, the variational form of the problem defined by Eqs. (9) and (10) is assumed to be [5]

$$\int_{\Omega} \boldsymbol{\Psi} \cdot \mathcal{R}(U)\, \mathrm{d}\Omega + \sum_{e} \int_{\Omega_e} \boldsymbol{P}(\boldsymbol{\Psi}) \cdot \mathcal{R}(U)\, \mathrm{d}\Omega_e + \int_{\Gamma_H} \boldsymbol{\Psi} \cdot [(K : L(U)) \cdot \boldsymbol{n} - H]\, \mathrm{d}\Gamma + \int_{\Gamma_*} \boldsymbol{\Psi} \cdot (U - U^*)\, \mathrm{d}\Gamma = 0 \tag{13}$$

3. Upwinding tensor computation

In order to obtain the 'upwinding tensor' $\boldsymbol{\tau}$, the following advection–diffusion system is considered

$$\boldsymbol{A} : \boldsymbol{L} - \boldsymbol{\nabla} \cdot (\boldsymbol{K} : \boldsymbol{L}) = \boldsymbol{0} \tag{14}$$

that is, in fact, system (3) neglecting the source term and assuming steady-state conditions.

Due to the geometric mapping from the parent domain to the elemental domain related to the isoparametric finite elements, Eq. (14) can be written in this local elemental system $\boldsymbol{\xi}$. Taking this fact into account, the following expression can be obtained

$$\boldsymbol{L}(\boldsymbol{U}) = L_{mn} = \frac{\partial U_m}{\partial x_n} = \frac{\partial U_m}{\partial \xi_r} \frac{\partial \xi_r}{\partial x_n} = \hat{L}_{mr} J_{rn} = \hat{\boldsymbol{L}}(\boldsymbol{U}) \cdot \boldsymbol{J} \tag{15}$$

where $\hat{\boldsymbol{L}}(\boldsymbol{U}) = \hat{L}_{mr} = \partial U_m / \partial \xi_r$ and $\boldsymbol{J} = J_{rn} = \partial \xi_r / \partial x_n$ is the Jacobian transformation matrix, with $r = 1, \ldots, n_{\dim}$.

With these considerations, the generalized convective term can be written as

$$\boldsymbol{A} : \boldsymbol{L}(\boldsymbol{U}) = A_{imn} L_{mn} = A_{imn} \hat{L}_{mr} J_{rn} = \hat{\boldsymbol{A}} : \hat{\boldsymbol{L}}(\boldsymbol{U}) \tag{16}$$

where $\hat{\boldsymbol{A}}$ is defined by

$$\hat{\boldsymbol{A}} = \hat{A}_{imr} = A_{imn} J_{rn} = \boldsymbol{A} \cdot \boldsymbol{J}^{\mathrm{T}} \tag{17}$$

that, for a fixed value $r = \bar{r}$, $\hat{\boldsymbol{A}}_{\bar{r}}$ is

$$\hat{\boldsymbol{A}}_{\bar{r}} = [\hat{A}_{im\bar{r}}] = \begin{bmatrix} \hat{a}_{\bar{r}} & 0 & 0 & J_{\bar{r}1} \\ 0 & \hat{a}_{\bar{r}} & 0 & J_{\bar{r}2} \\ 0 & 0 & \hat{a}_{\bar{r}} & J_{\bar{r}3} \\ J_{\bar{r}1} & J_{\bar{r}2} & J_{\bar{r}3} & 0 \end{bmatrix} \tag{18}$$

where $\hat{a}_{\bar{r}} = \rho L_{\bar{r}j} u_j$.

In this context, the generalized diffusion term is

$$\boldsymbol{\nabla} \cdot \boldsymbol{K} : \boldsymbol{L} = \nabla_j K_{jimn} L_{mn} = \hat{\nabla}_r J_{rj} K_{jimn} \hat{L}_{ms} J_{sn} = \hat{\nabla}_r \hat{K}_{rims} \hat{L}_{ms} = \hat{\boldsymbol{\nabla}} \cdot \hat{\boldsymbol{K}} : \hat{\boldsymbol{L}} \tag{19}$$

where $s = 1, \ldots, n_{\dim}$, $\hat{\nabla}_r(\cdot) = \partial(\cdot)/\partial \xi_r$, and

$$\hat{\boldsymbol{K}} = \hat{K}_{rims} = J_{rj} K_{jimn} J_{sn} = \boldsymbol{J} \cdot \boldsymbol{K} \cdot \boldsymbol{J}^{\mathrm{T}} \tag{20}$$

As mentioned before, Eq. (14) is written in the local system $\boldsymbol{\xi}$ as

$$\hat{\boldsymbol{A}} : \hat{\boldsymbol{L}} - \hat{\boldsymbol{\nabla}} \cdot \hat{\boldsymbol{K}} : \hat{\boldsymbol{L}} = \boldsymbol{0} \tag{21}$$

Moreover, the matrix-valued p-norm of $\hat{\boldsymbol{A}}$ is defined as [5]

$$|\hat{\boldsymbol{A}}|_p = \left\{ \sum_r |\hat{\boldsymbol{A}}_r|^p \right\}^{1/p} \tag{22}$$

such that p can be chosen in the integer interval $[1, \infty]$, and $|\hat{\boldsymbol{A}}_r|^p$ are obtained solving the $\hat{\boldsymbol{A}}_r$ eigenproblem as

$$|\hat{\boldsymbol{A}}_r|^p = {}^r\boldsymbol{T} \cdot |\boldsymbol{\Lambda}_{\hat{A}_r}|^p \cdot {}^r\boldsymbol{T}^{-1} = {}^rT_{iq} |{}^r\lambda_q|^p \, {}^rT^{-1}_{qm} \tag{23}$$

where $\boldsymbol{\Lambda}_{\hat{A}_r}$ is the diagonal tensor of the eigenvalues ${}^r\lambda_q$ of $\hat{\boldsymbol{A}}_r$ and ${}^rT_{iq}$ is the i component of the eigenvector associated with the qth eigenvalue. Notice that this eigenproblem has only real solution due to the symmetric form of $\hat{\boldsymbol{A}}_r$ as it can be seen in Eq. (18). Therefore, the calculation of $|\hat{\boldsymbol{A}}|_p$ is performed by Eq. (22) and its eigenproblem is solved as

$$|\hat{\boldsymbol{A}}|_p = \boldsymbol{Y} \cdot \boldsymbol{\Lambda} \cdot \boldsymbol{Y}^{-1} \tag{24}$$

where $\boldsymbol{\Lambda} = [\lambda_{c_q}]$ is the diagonal tensor of the eigenvalues of $|\hat{\boldsymbol{A}}|_p$ and $\boldsymbol{Y} = [Y_{iq}]$ are the eigenvectors associated to them. The upwinding tensor will be defined in the basis of these eigenvectors. Firstly, it is necessary to describe the generalized diffusion tensor in the eigenvector system of the matrix-valued p-norm of the generalized convective tensor (the $\boldsymbol{Y}$ system). This tensor is called $\bar{\boldsymbol{K}}$ and it is defined as

$$\bar{\boldsymbol{K}} = [\bar{\boldsymbol{K}}_{jn}] = \bar{K}_{jimn} = Y^{-1}_{iq} \hat{K}_{jqln} Y_{lm} \tag{25}$$

with $l = 1, \ldots, n_{\text{dim}} + 1$.

Further, a matrix-valued p-norm of $\bar{\boldsymbol{K}}$ is evaluated as

$$|\bar{\boldsymbol{K}}|_p = \left\{ \sum_j \sum_n |\bar{\boldsymbol{K}}_{jn}|^p \right\}^{1/p} \tag{26}$$

and $|\bar{\boldsymbol{K}}|_p$ is enforced to be diagonal in the $\boldsymbol{Y}$ system using a conventional lumped technique [13]. These diagonal values are called λ_{k_i}.

At this stage, the upwind coefficient in each direction of $\boldsymbol{Y}$ is calculated as

- $\tau_i = 0$ if $\lambda_{c_i} = 0$ (27.1)
- $\tau_i = \dfrac{\zeta(\alpha_i)}{\lambda_{c_i}}$ if $\lambda_{c_i} \neq 0$ and $\lambda_{k_i} \neq 0$ (27.2)
- $\tau_i = \dfrac{1.}{\lambda_{c_i}}$ if $\lambda_{c_i} \neq 0$ and $\lambda_{k_i} = 0$ (27.3)

where ζ is the nondimensional numerical diffusivity optimal function defined by [13]

$$\zeta(\alpha_i) = \coth(\alpha_i) - \alpha_i^{-1} \tag{27.4}$$

and α_i is the elemental Péclet number

$$\alpha_i = \frac{\lambda_{c_i}}{\lambda_{k_i}} \tag{27.5}$$

The 'upwinding tensor' in system $\boldsymbol{Y}$ is written as

$$\boldsymbol{\tau}_Y = \tau_{Y_{ij}} = \delta_{ik} \tau_k \delta_{kj} \tag{28}$$

where δ is the Kronecker delta. Finally, the upwinding tensor used in Eqs. (11) and (12) is obtained transforming back this last expression as

$$\boldsymbol{\tau} = \boldsymbol{Y} \cdot \boldsymbol{\tau}_Y \cdot \boldsymbol{Y}^{-1} \tag{29}$$

It should be noted that this methodology obviously satisfies the three designs conditions proposed by Hughes et al. [5]: (i) it reduces correctly to the optimal one-dimensional system case; (ii) it is equivalent to SUPG for a scalar, multidimensional advection–diffusion equation; and (iii) it reduces to SUPG on each uncoupled component of multidimensional simultaneously diagonalizable advection–diffusion system (this implies that ${}^{r}\boldsymbol{T}$ of Eq. (23) are the same for all r).

In particular, in the present work $p = 1$ is adopted in the computation of the p-norm.

4. Finite element formulation

In the framework of the finite element method [13] the continuous field of unknowns $\boldsymbol{U}$ are locally approximated by polinomial functions in the standard manner as

$$\boldsymbol{U} \simeq \boldsymbol{U}_h = \boldsymbol{\Phi}_h \hat{\boldsymbol{U}} \tag{30}$$

where $\boldsymbol{U}_h$ is the approximation of the continuous unknown vector $\boldsymbol{U}$, $\hat{\boldsymbol{U}}$ is the nodal unknown vector and $\boldsymbol{\Phi}_h$ are the typical shape functions for standard finite elements [13].

The spatial domain is discretized by a collection of n_{el} elements disjointed such that the union of them is the original domain. Therefore, the continuous variational form of the problem described in Eq. (13) can be written in a semidiscrete form as [5]

$$\begin{aligned}\boldsymbol{R} \equiv & \int_{\Omega} \boldsymbol{\Phi}_h \cdot \mathscr{R}(\boldsymbol{U}_h)\, \mathrm{d}\Omega + \sum_{e} \int_{\Omega_e} \boldsymbol{P}(\boldsymbol{\Phi}_h) \cdot \mathscr{R}(\boldsymbol{U}_h)\, \mathrm{d}\Omega_e \\ & + \int_{\Gamma_H} \boldsymbol{\Phi}_h \cdot [(\boldsymbol{K} : \boldsymbol{L}(\boldsymbol{U}_h)) \cdot \boldsymbol{n} - \boldsymbol{H}]\, \mathrm{d}\Gamma + \int_{\Gamma_*} \boldsymbol{\Phi}_h \cdot (\boldsymbol{U}_h - \boldsymbol{U}^*)\, \mathrm{d}\Gamma = \boldsymbol{0}\end{aligned} \tag{31}$$

where $\boldsymbol{\Phi}_h$ is adopted as the discrete form of the test function $\boldsymbol{\Psi}$ of Eq. (13) and $\boldsymbol{R}$ is the residual vector [13].

The temporal discretization of Eq. (31) has been done using the well-known Euler backward scheme [13].

5. Solution strategy

When the residual is differentiable, a Newton-type incremental-iterative formulation for solving the nonlinear semidiscrete system (31) can be attempted. This means that [13]

$${}^{t+\Delta t}\boldsymbol{J}^{j-1}\, \Delta \boldsymbol{U}^{j} = {}^{t+\Delta t}\boldsymbol{R}^{j-1}, \tag{32}$$

$${}^{t+\Delta t}\boldsymbol{U}^{j} = {}^{t+\Delta t}\boldsymbol{U}^{j-1} + \Delta \boldsymbol{U}^{j} \quad j = 1, \ldots, n_{\mathrm{iter}}; \tag{33}$$

$${}^{t+\Delta t}\boldsymbol{U}^{0} = {}^{t}\boldsymbol{U}, \tag{34}$$

where the iteration index j denotes the jth approximation to the solution in $t + \Delta t$ (the solution at time t is assumed to be known), and $\boldsymbol{J}$ is the tangent Jacobian matrix $\boldsymbol{J} = -\partial \boldsymbol{R} / \partial \boldsymbol{U}$.

The convergence criterion is written in terms of the norm of the residual vector in the following form

$$\frac{\|\boldsymbol{R}\|_{L_2}}{\|\boldsymbol{F}^*\|_{L_2}} \leq \varepsilon_r \tag{35}$$

where ε_r is the admissible tolerance (taken as 10^{-10} in this work), $\boldsymbol{F}^*$ is a reference vector (the residual in the prescribed degrees of freedom or the body force vector if it exists) and $\|\cdot\|_{L_2}$ is the standard L_2 vector norm [13].

6. Numerical examples

6.1. Driven cavity flow problem

This example is a classical test used by several authors in order to check the quality of the methodology employed. In the present analysis, two different boundary conditions at the top corners are considered (see Fig. 2). The velocity is fixed in the walls and the pressure is taken equal to zero in the middle of the bottom. In the domain, the initial value of the unknowns are adopted equal to zero for all the cases presented. The geometry of the problem, the boundary conditions, the characteristic lengths and the meshes used in this work are shown in Figs. 2 and 3.

The stationary problem is considered for different Reynolds' numbers. The numerical results are compared with those obtained by

(a) Ghia et al. [14], no upwind F.D.M., 128×128 elements (Re = 1000), 256×256 elements (Re = 5000, 10 000).
(b) Nallasamy and Prasad [15], upwind F.D.M., 50×50 elements (Re = 5000, 10 000).
(c) Fortin and Thomasset [16], F.E.M., 12×12 elements (Re = 1000).
(d) Bercovier and Engelman [17], no upwind F.E.M. with penalization, 12×12 elements (Re = 1000).
(e) Kondo et al. [18], third-order upwind F.E.M., 40×40 elements (Re = 1000), 44×44 elements (Re = 10 000).
(f) Tanahashi et al. [19], GSMAC F.E.M.

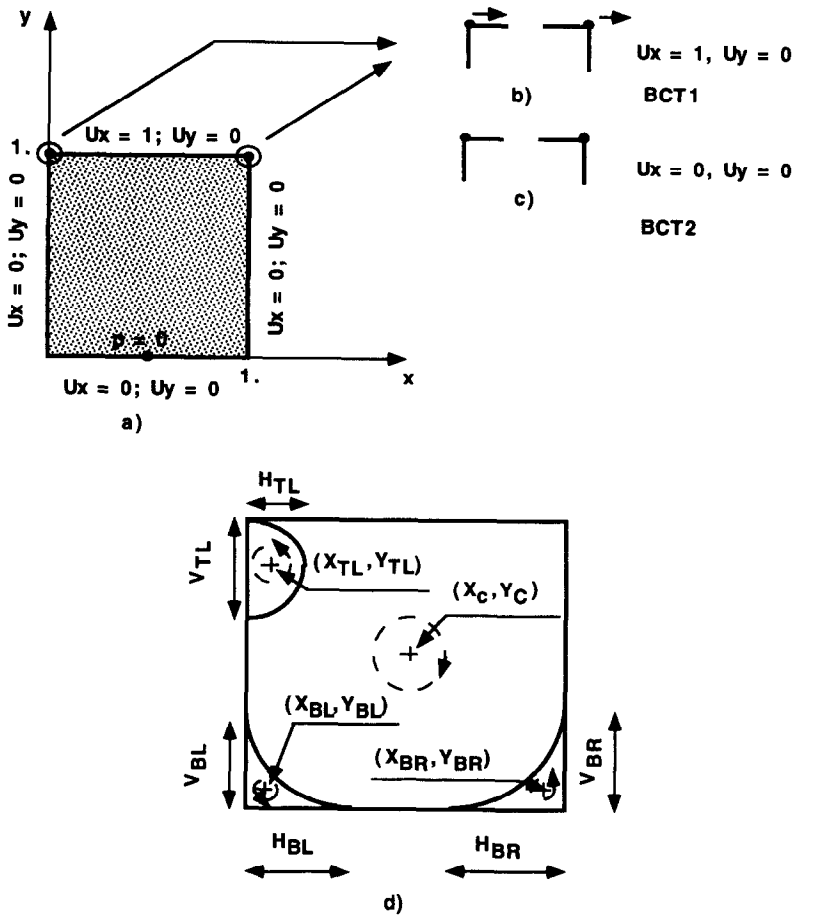

Fig. 2. Driven cavity flow. (a) Geometry; (b) boundary condition type 1 (BCT1); (c) boundary condition type 2 (BCT2); (d) characteristic lengths.

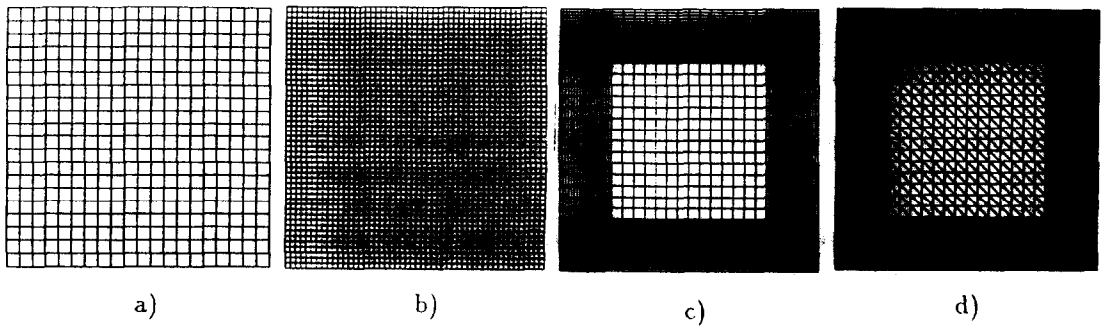

Fig. 3. Driven cavity flow—Finite element meshes: (a) uniform, 400 four-noded elements; (b) uniform, 2500 four-noded elements; (c) nonuniform, 2500 four-noded elements; (d) nonuniform, 5000 three-noded elements.

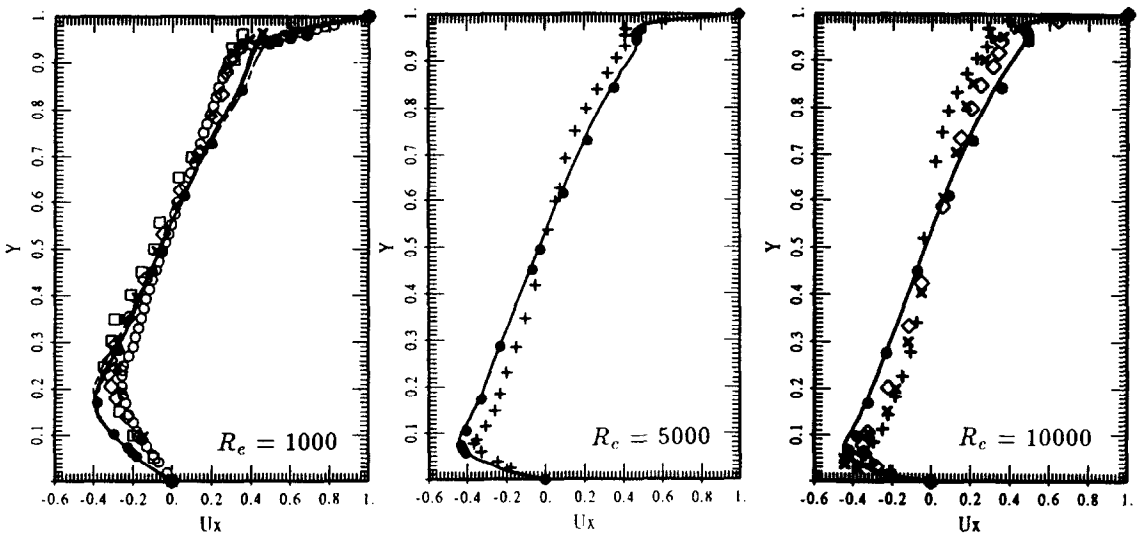

Fig. 4. Horizontal velocity profile for cavity flow at different Reynolds' numbers along the line $x = 0.5$ with BCT2: ●, Ghia et al. [14]; ×, Nallasamy [15]; □, Fortin and Thomasset [16]; ○, Bercovier and Engelman [17]; ◇, Kondo et al. [18]; +, Tanahashi et al. [19]. Present work: ——— mesh (a); – – – mesh (b); —— mesh (c); ———— mesh (d).

Table 1
Re = 1000—Steady-state analysis

	Tanahashi et al. [19]	Ghia et al. [14]	Present work
x_c	0.5335	0.5313	0.5409
y_c	0.5653	0.5625	0.5855
x_{BR}	0.8672	0.8594	0.8684
y_{BR}	0.1119	0.1094	0.1072
x_{BL}	0.0822	0.0859	0.0760
y_{BL}	0.0731	0.0781	0.0754
H_{BR}	0.3091	0.3034	0.3099
V_{BR}	0.3410	0.3536	0.3710
H_{BL}	0.2045	0.2188	0.2076
V_{BL}	0.1523	0.1680	0.1826

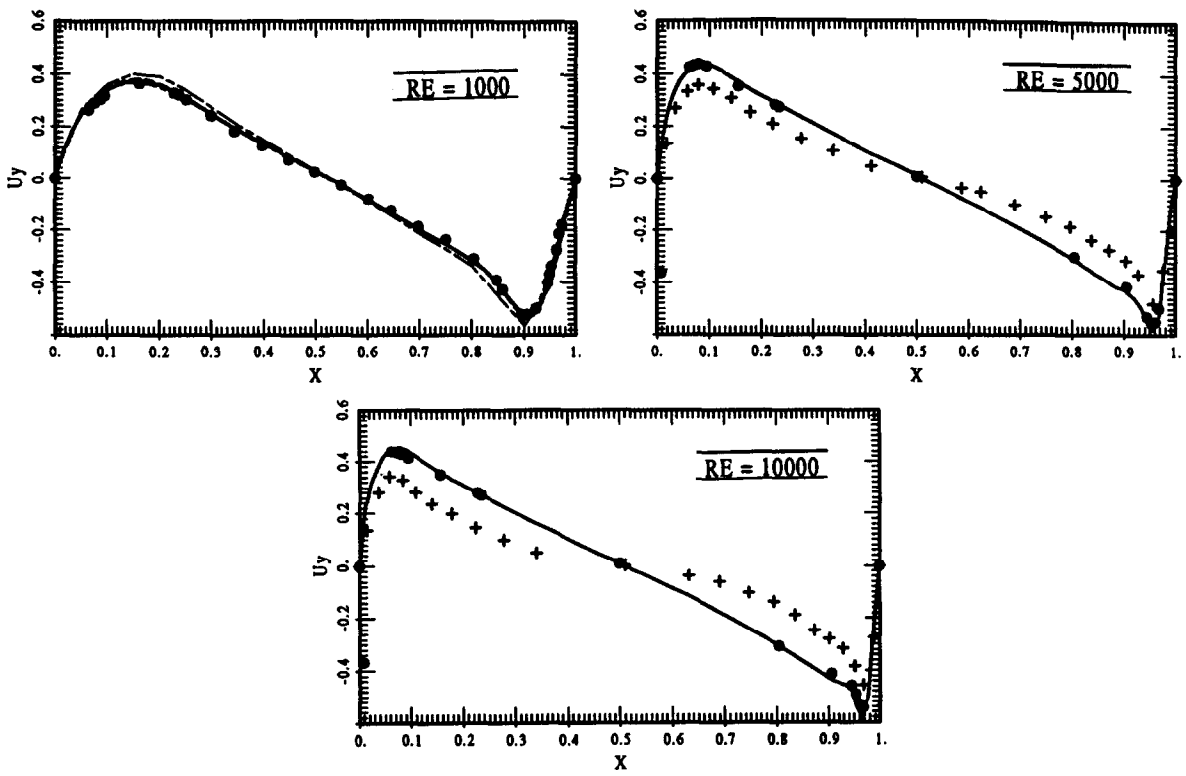

Fig. 5. Distribution of y-component of the velocity at different Reynolds' numbers along the line $y = 0.5$ for cavity flow with BCT2: ●, Ghia et al. [14]; + Tanahashi et al. [19]. Present work at Re = 1000: ——— mesh (a); – – – mesh (b); —— mesh (c); ——— mesh (d). Present work at Re = 5000 and 10 000: —— mesh (c).

Fig. 4 shows the horizontal velocity profile along the line $x = 0.5$ for Re = 1000, 5000 and 10 000 and the corresponding comparison with other authors. The top velocity boundary condition used is type 2 (see Fig. 2). In addition, the vertical velocity profile along the line $y = 0.5$ is plotted in Fig. 5. The results obtained in the present work using different meshes are in very good agreement with Ghia et al. [14].

The characteristic lengths obtained with the present formulation are compared with the results of other authors and are shown in Tables 1–3 for Re = 1000, Re = 5000 and Re = 10 000, respectively.

Table 2
Re = 5000—Steady-state analysis

	Tanahashi et al. [19]	Ghia et al. [14]	Present work
x_c	0.5120	0.5117	0.5029
y_c	0.5337	0.5352	0.5420
x_{BR}	0.8134	0.8086	0.8012
y_{BR}	0.0753	0.0742	0.0638
x_{BL}	0.0750	0.0703	0.0754
y_{BL}	0.1318	0.1367	0.1345
x_{TL}	0.0658	0.0625	0.0585
y_{TL}	0.9045	0.9102	0.9130
H_{BR}	0.3496	0.3565	0.3623
V_{BR}	0.4350	0.4180	0.4145
H_{BL}	0.3159	0.3184	0.2923
V_{BL}	0.2693	0.2643	0.2840
H_{TL}	0.1208	0.1211	0.1101
V_{TL}	0.2555	0.2693	0.2923

Table 3
Re = 10 000—Steady-state analysis

	Tanahashi et al. [19]	Ghia et al. [14]	Present work
x_c	0.5125	0.5117	0.5000
y_c	0.5274	0.5333	0.5420
x_{BR}	0.7944	0.7656	0.7573
y_{BR}	0.0640	0.0586	0.0551
x_{BL}	0.0790	0.0586	0.0676
y_{BL}	0.1400	0.1641	0.1536
x_{TL}	0.0758	0.0703	0.0676
y_{TL}	0.9120	0.9141	0.9130
H_{BR}	0.3773	0.3906	0.3655
V_{BR}	0.4529	0.4492	0.4522
H_{BL}	0.3515	0.3438	0.3216
V_{BL}	0.2834	0.2891	0.2899
H_{TL}	0.1683	0.1589	0.1491
V_{TL}	0.3463	0.3203	0.3333

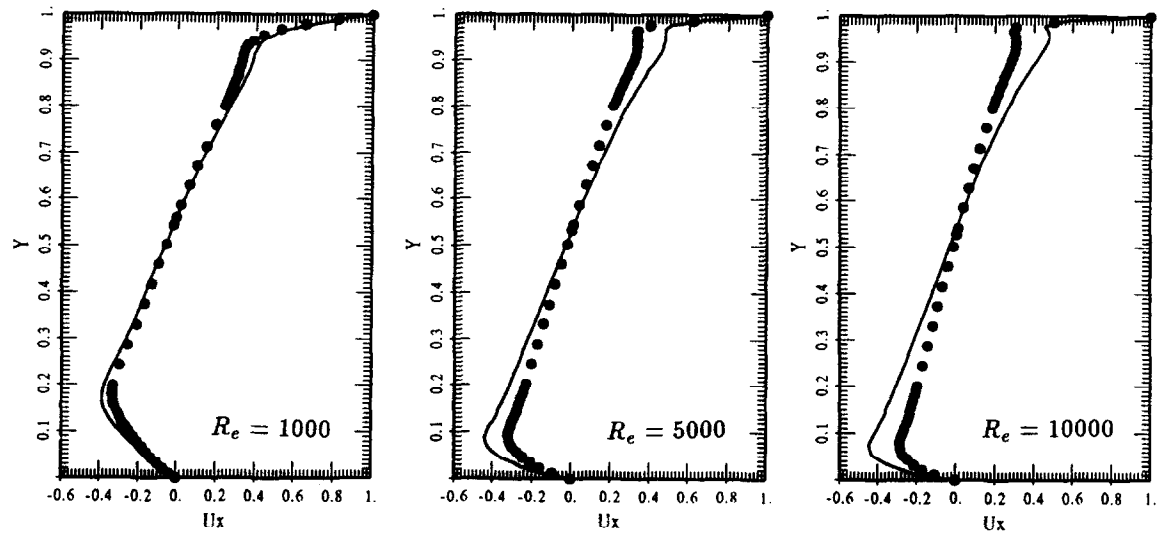

a) x-component of the velocity along the line $x = 0.5$.

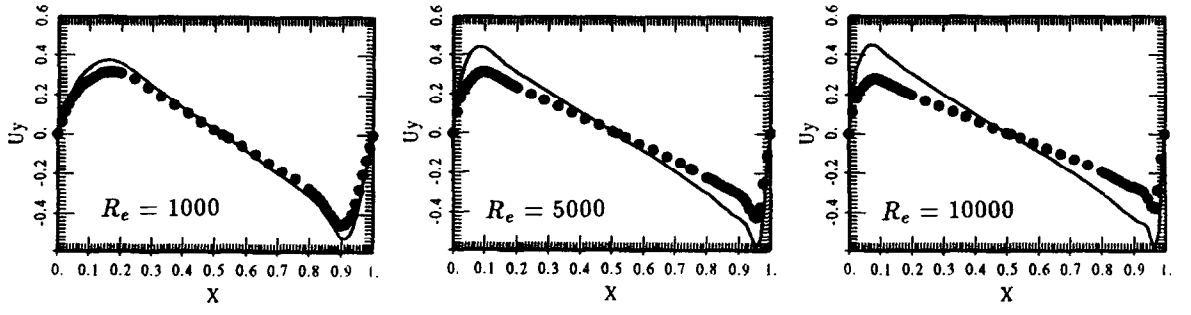

b) y-component of the velocity along the line $y = 0.5$.

Fig. 6. Driven cavity flow problem—BCT1 (●) in comparison with BCT2 (—) at different Reynolds' numbers with the formulation presented in this work using mesh (c).

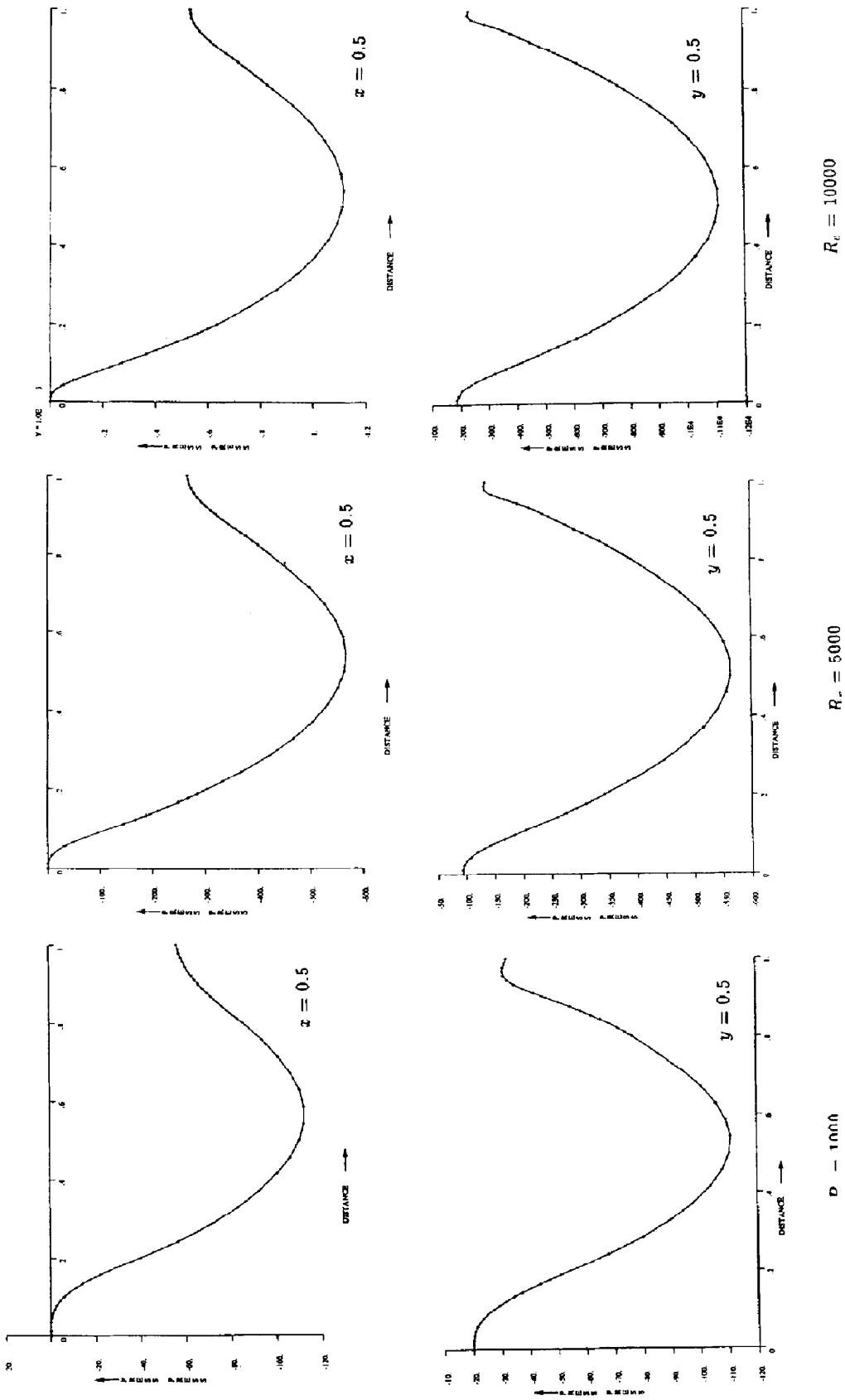
x = 0.5
y = 0.5
DISTANCE
$R_e = 10000$
$R_e = 5000$
$R_e = 1000$

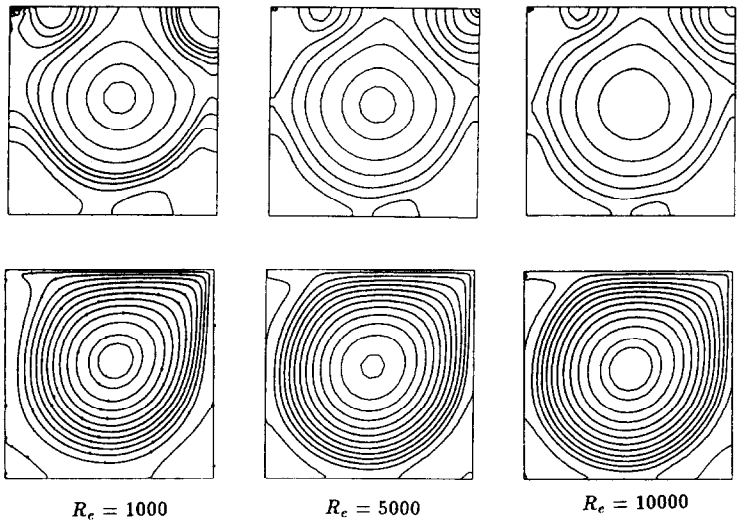

Fig. 8. Cavity flow problem—Pressure contours and streamlines.

The effect of the top boundary condition at different Reynolds' numbers is presented in Fig. 6.

The results obtained for Re = 1000, 5000 and 10 000 using a scalar upwinding GLS-type technique [11,12] are similar to those computed using the present methodology with the same numerical strategy.

The pressure profile along the lines $x = 0.5$ and $y = 0.5$ are plotted for different Reynolds' numbers in Fig. 7. It is seen that there are not oscillations in these profiles. Fig. 8 shows the streamline and pressure contours at different Reynolds' numbers. Once more, the numerical response does not present significant oscillations.

In addition, the values for the streamline function (ψ) are presented in Tables 4–6 for the Reynolds'

Table 4
Re = 1000—Steady-state analysis. Streamvalues

	Ghia et al. [14]	Present work
ψ_c	−0.117929	−0.118
ψ_{BR}	$1.75102\,10^{-3}$	$1.75\,10^{-3}$
ψ_{BL}	$2.31129\,10^{-4}$	$2.25\,10^{-4}$

Table 5
Re = 5000—Steady-state analysis. Streamvalues

	Ghia et al. [14]	Present work
ψ_c	−0.118966	−0.1215
ψ_{BR}	$3.08358\,10^{-3}$	$3.27\,10^{-3}$
ψ_{BL}	$1.36119\,10^{-3}$	$1.3\,10^{-3}$
ψ_{TL}	$1.45641\,10^{-3}$	$1.29\,10^{-3}$
$\psi_{BR_{(2)}}$	$-1.43226\,10^{-6}$	$-1.6\,10^{-6}$

Table 6
Re = 10 000—Steady-state analysis. Streamvalues

	Ghia et al. [14]	Present work
ψ_c	−0.119731	−0.1197
ψ_{BR}	$3.41831\,10^{-3}$	$3.79\,10^{-3}$
ψ_{BL}	$1.51829\,10^{-3}$	$1.38\,10^{-3}$
ψ_{TL}	$2.42103\,10^{-3}$	$2.3\,10^{-3}$
$\psi_{BR_{(2)}}$	$-1.31321\,10^{-4}$	$-2.3\,10^{-4}$

Table 7
Vorticity values

Re	Ghia et al. [14]	Present work
1000	2.04968	2.07
5000	1.86016	1.9
10 000	1.88082	1.8

numbers 1000, 5000 and 10 000, respectively. The vorticity values in the main vortex at different Reynolds' numbers are presented in Table 7.

6.2. Backward-facing step flow problem

The backward-facing step flow problem is a very interesting test in order to compare the numerical results with the experimental ones obtained by Armaly et al. [20]. In the present analysis, the effect of the gravity action (in the vertical direction) is taking into account in order to reproduce the experimental test. The geometry and the characteristic lengths defined in this problem [20] are plotted in Fig. 9. A regular (structured) mesh composed of nearly 9000 four-noded bilinear isoparametric elements have been used in the computations. The velocity is prescribed to zero in the channel walls and a parabolic profile with maximum velocity V_{max} is considered at the inlet face. The velocity field is not restricted at the exit. The pressure is zero at the top corner in the outlet face. The air properties are taken as $\mu = 0.000018$ for the dynamic viscosity and $\rho = 1.2$ for the density (all in consistent units). The Reynolds' numbers are computed from the maximum inlet velocities (V_{max}) and the hydraulic diameter of the inlet channel (D) as $\mathrm{Re} = (2V_{max}D\rho)/(3\mu)$ [21]. The streamline and the velocity contours are presented in Fig. 10. In Table 8 the numerical results obtained in the present work and the experimental ones [20] are presented. It is possible to achieve convergence for high Reynolds' numbers but the disagreement between the experimental and numerical results, in particular for Re = 1600, can be due to the laminar numerical model used. Other reasons for these differences is the effect of the three dimensionality in the experimental results [20]. On the other hand, the numerical results are similar to that obtained in [21] using a traditional SUPG method with penalization and applying a continuation technique: 10.3, 10.8 and 17.2 for x_i/s, $i = 1, 2, 3$ at Re = 800; and 12.8, 13.0 and 22.1 for the same characteristic lengths at Re = 1000. Fig. 11 shows the pressure contours under the gravity action. It should be noted that vertical isopressure lines near the inlet and the outlet would be obtained if the gravity action is not considered [21]. Finally, the same analysis have been performed in [11,12] using a scalar upwinding GLS technique leading to similar results in comparison with those obtained using the present formulation.

6.3. Two-liquid interface problem

This problem has also been analysed in [22] and [10]. Two liquids with the same dynamic viscosity and different densities equal to 1.0 and 2.0, respectively, occupy a closed tank with dimensions 0.8×0.6

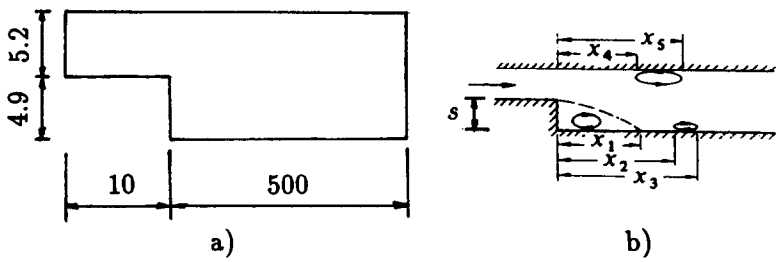

Fig. 9. Backward-facing step flow. (a) Geometry (out of scale) in mm and (b) characteristic lengths.

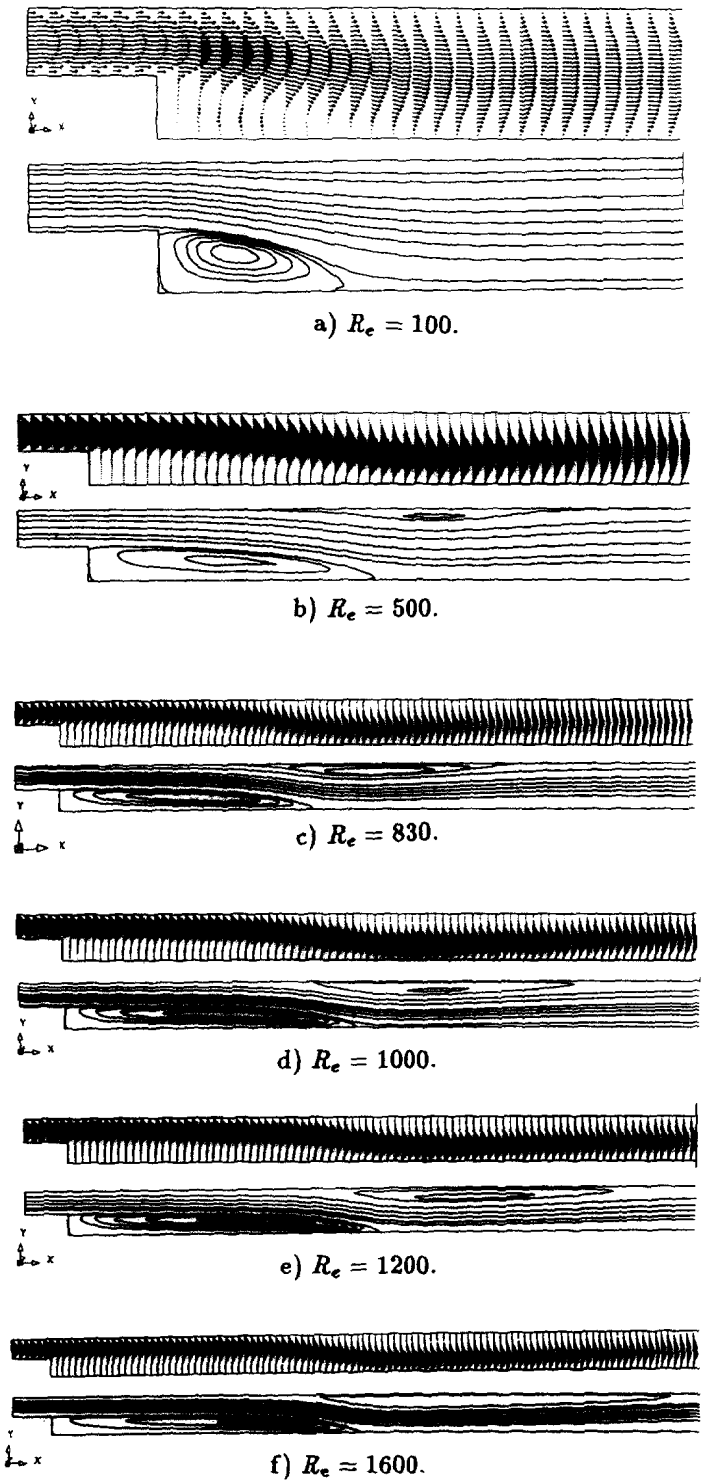

Fig. 10. Backward-facing step flow—Velocity profile and streamlines for different Reynolds' numbers.

Table 8
Backward-facing step flow at different Reynolds' numbers

	Re	x_1/s	x_4/s	x_5/s
Present work	100	3.0		
Armaly et al. [20]	100	3.0		
Present work	500	8.5	8.0	12.8
Armaly et al. [20]	500	10.0	8.0	13.5
Present work	830	11.5	10.5	19.4
Armaly et al. [20]	830	14.0	11.25	20.0
Present work	1000	12.93	11.22	22.79
Armaly et al. [20]	1000	16.25	13.5	21.8
Present work	1200	14.6	13.3	25.5
Armaly et al. [20]	1200	17.6	14.5	23.5
Present work	1600	17.0	14.6	34.0
Armaly et al. [20]	1600	13.9	9.5	22.0

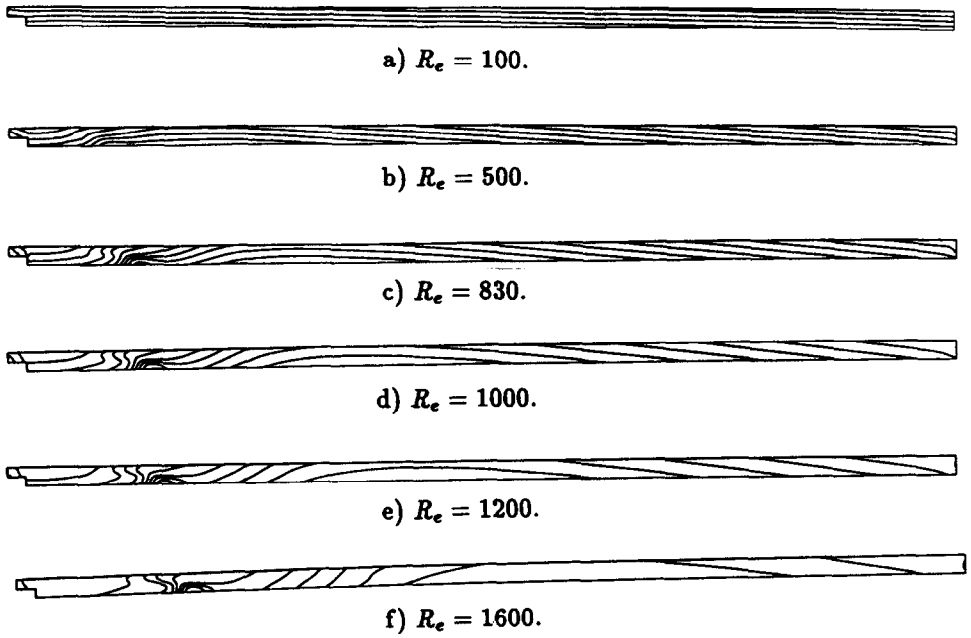

Fig. 11. Backward-facing step flow—Pressure contours.

(all in consistent units). The initial interface position is linear with a slope of 0.25 and average height of 0.3. The lighter liquid is on top of the heavier one and the gravity is 0.294. The analysis performed is transient with a time step equal to 0.5. The geometry and the four-noded finite element mesh used are shown in Fig. 12. The normal velocity is prescribed equal to zero in all sides of the tank while the tangencial component is set to zero at the top and bottom sides (BCT1). The pressure is taken equal to zero at the top right corner. The interface position is obtained using the methodology developed in [23], consisting in following the interface by means of an arbitrary lagrangian mesh using the total velocity of the fluid particles belonging to it. The vertical location of the interface along the sides of the tank are plotted in Fig. 13. A very good agreement with the results obtained by Tezduyar et al. [22] can be observed. The pressure at different time steps are shown in Fig. 14. Once more, these results are very similar to those obtained in [22]. The results obtained prescribing only the normal velocity to zero on the top and bottom sides of the tank (BCT2) are plotted in Fig. 15 and they are compared with the results computed using the present methodology with BCT1. Fig. 16 shows the results obtained with the methodology presented in this work and those computed with a scalar upwinding GLS-type techniques

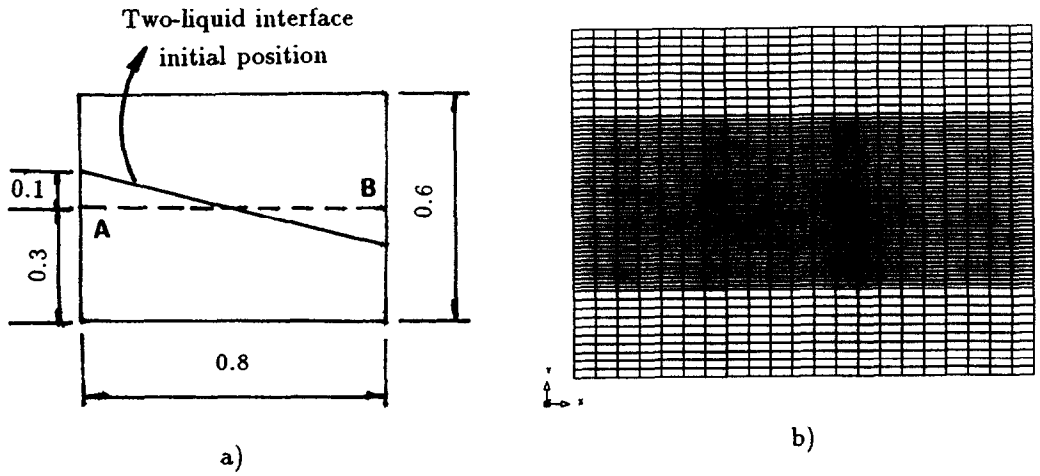

Fig. 12. Two-liquid interface—Geometry (a) and four-noded finite element mesh (b).

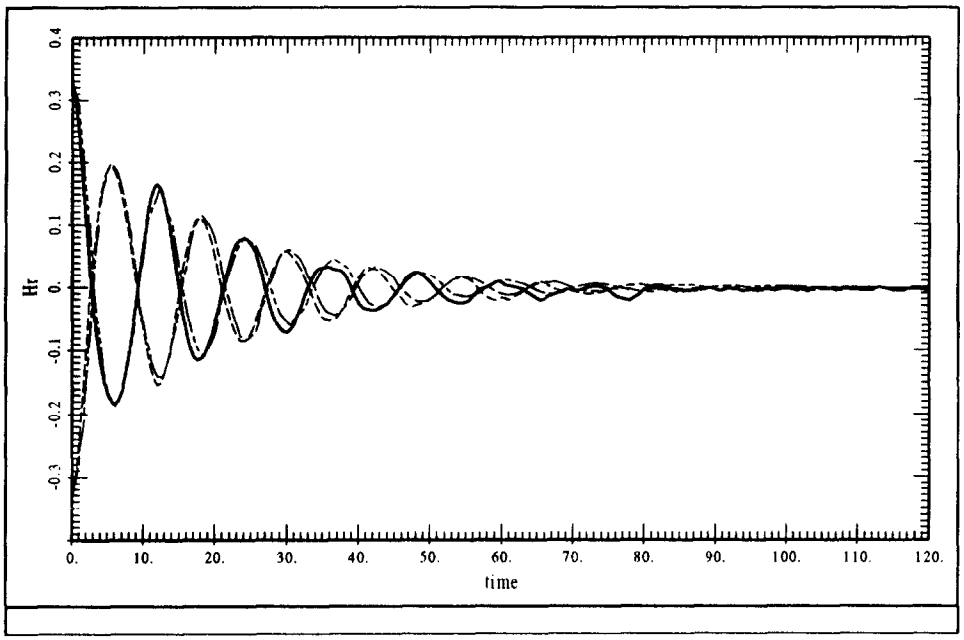

Fig. 13. Two-liquid interface—Time history of the interface positions in side A and side B of the tank. Side A: ——, Tezduyar et al. [22]; ——, present work. Side B: ——, Tezduyar et al. [22], ——, present work. (H_r = (wave height − 0.3)/0.3).

[11,12] (using in both cases BCT1 and the same numerical strategy). Note that in the second case there are difficulties to reach the incompressibility condition.

7. Conclusions

A finite element GLS type formulation for solving the incompressible Navier–Stokes flow equations has been developed. In this context, the state variables of the problem are the velocity and pressure. This new methodology is based on the generalized streamline operator including the definition of an upwinding tensor which does not require input tuning parameters. Another features of this technique

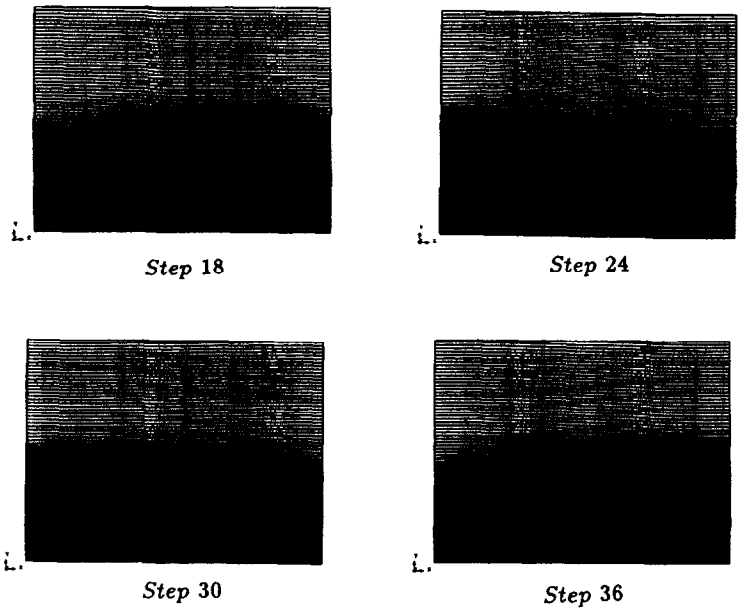

Fig. 14. Two-liquid interface—Pressure contours.

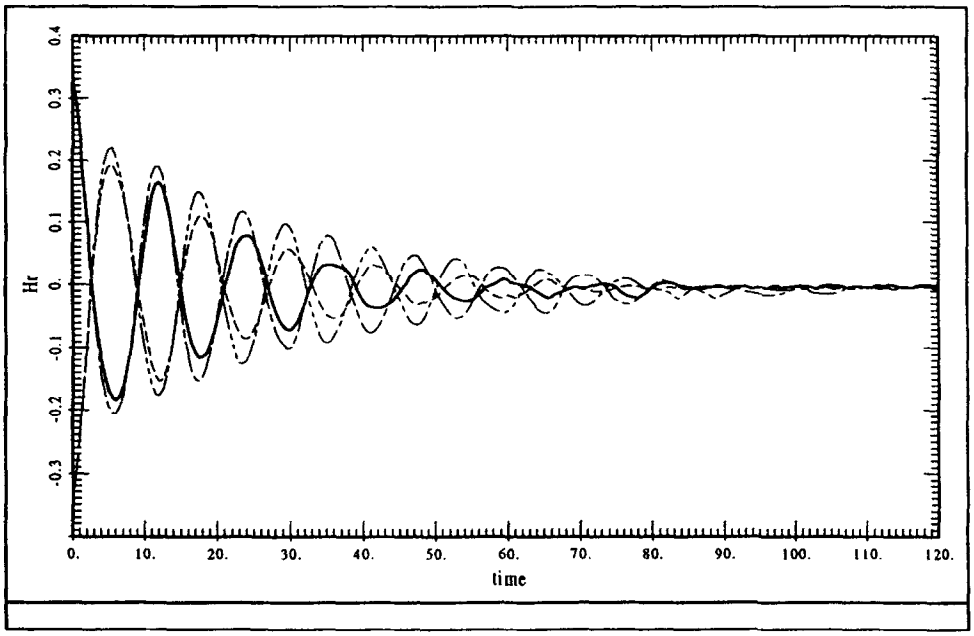

Fig. 15. Two-liquid interface—Time history of the interface positions in side A and side B of the tank. Side A: ——, BCT1; — — —, BCT2. Side B: – – –, BCT1; — — — —, BCT2. (H_r = (wave height − 0.3)/0.3).

are: it allows the use of equal order interpolation for velocity and pressure, no penalization methods are needed to satisfy the incompressibility condition and it reduces to the standard SUPG method for some particular cases related to the upwinding design conditions. Moreover, this formulation has been solved using a Newton-type incremental-iterative numerical scheme where the convergence criterion is written in terms of the residual vector. Finally, the numerical examples presented show a good agreement between the results obtained using the present formulation with some experimental measurements and other numerical results reported by different authors.

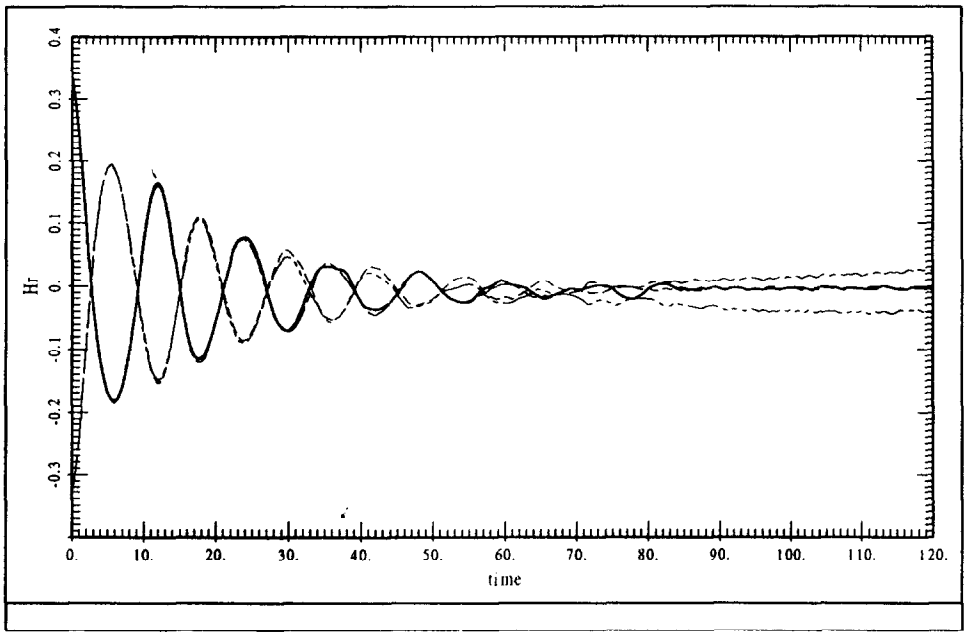

Fig. 16. Two-liquid interface—Time history of the interface positions in side A and side B of the tank. Side A: ——, Present work; — — —, Cruchaga and Oñate [19, 20]. Side B: – – –, Present work; — — — —, Cruchaga and Oñate [11, 12]. (H_r = (wave height − 0.3)/0.3).

Acknowledgment

The first author thanks Francisco Armero for many useful discussions related with some specific topics of this work.

References

[1] T.J.R. Hughes, L.P. Franca and M. Balestra, A new finite element formulation for computational fluid dynamics: V. Circumventing the Babuska–Brezzi condition: a stable Petrov–Galerkin formulation of the stokes problem accommodating equal-order interpolations, Comput. Methods Appl. Mech. Engrg. 59 (1986) 85–99.

[2] T.J.R. Hughes, L.P. Franca and G.M. Hulbert, A new finite element formulation for computational fluid dynamics: VIII. The Galerkin/least-squares method for advective–diffusive equations, Comput. Methods Appl. Mech. Engrg. 73 (1989) 173–189.

[3] O.C. Zienkiewicz and J. Wu, Incompressibility without tears—How to avoid restrictions of mixed formulation, Int. J. Numer. Methods Engrg. 32 (1991) 1189–1203.

[4] L.P. Franca and T.J.R. Hughes, Convergence analyses of Galerkin least-squares methods for symmetric advective–diffusive forms of the Stokes and incompressible Navier–Stokes equations, Comput. Methods Appl. Mech. Engrg. 105 (1993) 285–298.

[5] T.J.R. Hughes and M. Mallet, A new finite element formulation for computational fluid dynamics: III. The generalized streamline operator for multidimensional advective–diffusive systems, Comput. Methods Appl. Mech. Engrg. 58 (1986) 305-328.

[6] T.E. Tezduyar, M. Behr and J. Liou, A new strategy for finite element computations involving moving boundaries and interfaces—The deforming-spatial-domain/space–time procedure: I. The concept and the preliminary numerical tests, Comput. Methods Appl. Mech. Engrg. 94 (1992) 339–351.

[7] P.A.B. De Sampaio, A Petrov–Galerkin formulation for the incompressible Navier–Stokes equations using equal order interpolation for velocity and pressure, Int. J. Numer. Methods Engrg. 31 (1991) 1135–1149.

[8] M. Storti, N. Nigro and S. Idelsohn, Stabilizing equal-order interpolations for mixed formulations of Navier–Stokes equations via SUPG method, Internal report.

[9] G. Hauke and T.J.R. Hughes, A unified approach to compressible and incompressible flows, Comput. Methods Appl. Mech. Engrg. 113 (1994) 389–395.

[10] M.A. Cruchaga and E. Oñate, A finite element formulation for incompressible flow with moving surfaces using a generalized streamline operator, Proc. Ninth International Conference on Finite Elements in Fluids, 1995.
[11] M.A. Cruchaga and E. Oñate, A numerical solution strategy for the incompressible Navier–Stokes equations. Modeling and simulation, Proc. 1994 European Simulation Multiconference (1994) 699–703.
[12] M.A. Cruchaga and E. Oñate, Modelización por elementos finitos de las ecuaciones de Navier–Stokes para flujo incompresible mediante técnicas GLS, Mecánica computacional, ed. (AMCA, Santa Fe, Argentina) 14 (1994) 255–267.
[13] O.C. Zienkiewicz and R.L. Taylor, The Finite Element Method, Fourth edition (McGraw-Hill Book Company).
[14] U. Ghia, K.N. Ghia and C.T. Shin, High-Re solutions for incompressible flow using the Navier–Stokes equation and multigrid method, J. Comput. Phys. 48 (1982) 387–411.
[15] M. Nallasamy and K.K. Prasad, On cavity flow at high Reynolds numbers, J. Fluid Mech. 79 (1977) 391–414.
[16] M. Fortin and F. Thomasset, Mixed finite element methods for incompressible flow problems, J. Comput. Phys. 31 (1979) 113–145.
[17] M. Bercovier and M. Engelman, A finite element for the numerical solution of viscous incompressible flows, J. Comput. Phys. 30 (1979) 181–201.
[18] N. Kondo, T. Tosaka and T. Nishimura, High Reynolds solutions of the Navier–Stokes equations using the third-order upwind finite element method, Proc. Computacional Methods in Flow Analysis (Okayama, 1988) 984–911.
[19] T. Tanaheshi, H. Okanaga and T. Saito, GSMAC Finite Element Method for unsteady incompressible Navier–Stokes equations at high Reynolds numbers, Int. J. Numer. Methods in Fluids 11 (1990) 479–499.
[20] B.F. Armaly, F. Durst, J.C.F. Pereira and B. Schönung, Experimental and theoretical investigation of backward-facing step flow. J. Fluid Mech. 127 (1983) 473–496.
[21] R. Codina, A Finite Element model for incompressible flow problems, Doctoral Thesis, Barcelona, June, 1992.
[22] T.E. Tezduyar, M. Behr and J. Liou, A new strategy for finite element computations involving moving boundaries and interfaces. The deforming-spatial-domain/space–time procedure: II. Computation of free-surface flows two-liquid flows, and flows with drifting cylinders. Comput. Methods Appl. Mech. Engrg. 94 (1992) 339–351.
[23] M. Cruchaga, E. Oñate and S. Idelsohn, On the pseudomaterial approach for the analysis of transient forming processes, Comput. Numer. Methods Engrg. 11 (1995) 137–148.